JCI The Journal of Clinical Investigation

Selective disruption of TLR2/MyD88 interaction inhibits inflammation and attenuates Alzheimer's pathology

Suresh B. Rangasamy, … , David A. Bennett, Kalipada Pahan

J Clin Invest. 2018. https://doi.org/10.1172/JCI96209.

Research In-Press Preview Inflammation Neuroscience

Graphical abstract

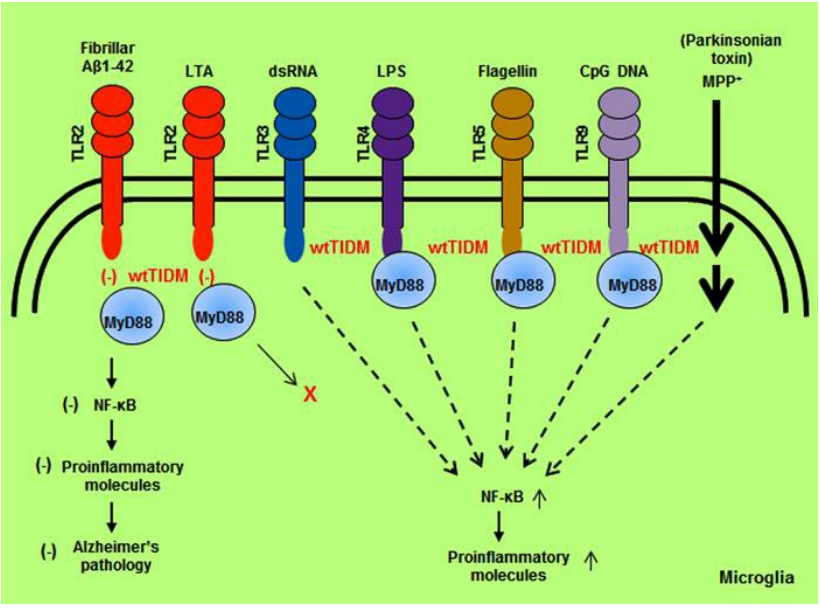

Find the latest version:

https://jci.me/96209/pdf

Selective disruption of TLR2/MyD88 interaction inhibits inflammation and attenuates Alzheimer's pathology

Suresh B. Rangasamy[1,*], Malabendu Jana[1,*], Avik Roy[1,*], Grant T. Corbett[1,*,&], Madhuchhanda Kundu[1], Sujyoti Chandra[1], Susanta Mondal[1], Sridevi Dasarathi[1], Elliott J. Mufson[2], Rama K. Mishra[3], Chi-Hao Luan[4], David A. Bennett[5], and Kalipada Pahan[1,6]

[1]Department of Neurological Sciences, Rush University Medical Center, Chicago, IL; [2]Barrow Neurological Institute, Phoenix, AZ; [3]Medicinal and Synthetic Chemistry Core, Center for Molecular Innovation and Drug Discovery, Northwestern University, Evanston, IL**;** [4]High Throughput Analysis Laboratory and Department of Molecular Biosciences, Northwestern University, Evanston, IL; [5]Rush Alzheimer's Disease Center, Rush University Medical Center, Chicago, IL; [6]Division of Research and Development, Jesse Brown Veterans Affairs Medical Center, 820 South Damen Avenue, Chicago, IL

[*]First four authors have equal contribution to the work.

[&]Current address: Ann Romney Center for Neurologic Diseases, Brigham and Women's Hospital, Harvard Medical School, Boston, MA

Conflict of interest: None

Running title: Selective inhibition of TLR2 activation by TIDM peptide

Corresponding author with complete address:
Kalipada Pahan, Ph.D.
Department of Neurological Sciences
Rush University Medical Center
1735 West Harrison St, Suite 310
Chicago, IL 60612
Tel: (312) 563-3592
Fax: (312) 563-3571
Email: Kalipada_Pahan@rush.edu

Abstract

Induction of TLR2 activation depends on its association with adapter protein MyD88. We have found that levels of TLR2 and MyD88 are elevated in the hippocampus and cortex of Alzheimer's disease (AD) patients and 5XFAD mouse model of AD. Since there is no specific inhibitor of TLR2, to target induced TLR2 from therapeutic angle, we engineered a peptide corresponding to the TLR2-interacting domain of MyD88 (TIDM) that binds to the BB loop of only TLR2, but not other TLRs. Interestingly, wild type (wt) TIDM peptide inhibited microglial activation induced by fibrillar Aβ1-42 and lipoteichoic acid, but not 1-methyl-4-phenylpyridinium, double-stranded RNA, bacterial lipopolysaccharide, flagellin, and CpG DNA. After intranasal administration, wtTIDM peptide reached the hippocampus, reduced hippocampal glial activation, lowered Aβ burden, attenuated neuronal apoptosis, and improved memory and learning in 5XFAD mice. However, wtTIDM peptide was not effective in 5XFAD mice lacking TLR2. In addition to 5XFAD mice, wtTIDM peptide also suppressed the disease process in mice with experimental allergic encephalomyelitis and collagen-induced arthritis. Therefore, selective targeting of activated status of one component of the innate immune system by wtTIDM peptide may be beneficial in AD as well as other disorders in which TLR2-MyD88 signaling plays a role in disease pathogenesis.

Introduction

Alzheimer's disease (AD) is the most common human neurodegenerative disorder that leads to memory loss. It is widely believed that AD is a multifactorial disorder affected by a mix of genetic, environmental, and lifestyle factors (1-3). Neuropathologically, AD is characterized by the presence of senile plaques and neurofibrillary tangles (NFT) (4-6). A number of studies (7-13) also suggest that glial activation and associated inflammation play an important role in

disease pathogenesis and that regulation of neuroinflammation may have therapeutic interest in attenuating neurodegeneration in AD.

Toll-like receptors (TLRs) serve as important links between innate and adaptive immunity primarily by responding to bacteria, bacterial products, viruses, viral products, and flagellin (14, 15). Currently, 11 different TLRs have been reported to exist in human and all the major CNS cell types are known to express TLRs (15, 16). However, microglia are the only cells in the CNS that express nearly all the TLRs known to date (16). Aside from TLR3, every TLR requires MyD88 for downstream signaling (14, 15). We (17) and others (18, 19) have shown that fibrillar Aβ peptides require TLR2 for microglial inflammation. Here, we demonstrated that levels of TLR2 and MyD88 increased *in vivo* in the frontal cortex and hippocampus of AD patients and 5XFAD mice. Since no option is available for specific targeting of induced TLR2, we designed a peptide corresponding to the TLR2-interacting domain of MyD88 (TIDM) that specifically inhibited induced TLR2 signaling and fibrillar Aβ-mediated microglial inflammation without modulating double-stranded RNA-, bacterial LPS-, flagellin-, CpG DNA-, and 1-methyl-4-phenylpyridinium (MPP^+)-mediated microglial activation. Moreover, intranasal administration of TIDM peptide resulted in reduction in hippocampal microglial activation, lowering of Aβ load, suppression of neuronal apoptosis, and improvement of memory and learning in 5XFAD mice, highlighting therapeutic promise of TIDM peptide in AD.

Results

Upregulation of TLR2 in AD: To investigate the role of TLR2 in the pathogenesis of AD, we monitored the level of TLR2 by immunoblot analysis in prefrontal cortex (PFC; Brodmann area 9) from 33 subjects who died with AD dementia (n=10), mild cognitive impairment (MCI; n=11) and age-matched individuals with no cognitive impairment (NCI; n=12) (table S1). In terms of age, sex, postmortem interval, brain weight, or Braak scores, no significant difference was found

across the groups (table S1). For comparison, we included TLR4. Since all the TLRs except TLR3 employ MyD88, we also investigated MyD88. Levels of both TLR2 and MyD88 in PFC were significantly altered between groups, with AD cases expressing more TLR2 and MyD88 relative to NCI and MCI cases (Fig. 1A-C & table S2). In contrast, TLR4 level did not significantly differ across the groups (Fig. 1A & D; table S2). The Spearman rank-order correlation showed that both TLR2 and MyD88 levels in prefrontal cortex were positively correlated with Braak staging (Fig. 1E-F & table S2). On the other hand, we did not find any relationship between TLR4 and Braak score (Fig. 1G & table S2). Importantly, MyD88 was also negatively correlated with mini-mental state examination (MMSE) and global cognitive z score (GCS) (Fig. 1H-M & table S2).

To confirm these findings, we performed double-label immunofluorescence analysis of hippocampal sections. As expected, the level of Iba-1 (microglial marker) was higher in the cortex and hippocampus of AD as compared to NCI (fig. S1A-E). Similar to Western blot results, we observed greater levels of TLR2 (fig. S1A & Fig. 1N-O) and MyD88 (fig. S1B & Fig. 1P-Q) in the cortex and hippocampus of AD brain compared with NCI. Again, there was no difference in TLR4 expression (fig. S1C & Fig. 1R-S).

Upregulation of TLR2 in 5XFAD transgenic (Tg) mice: Next, we examined the status of TLR2 and MyD88 in the hippocampus of 5XFAD Tg mice. Similar to that observed in the CNS of AD subjects, we noticed higher levels of TLR2 (fig. S2A-B) and MyD88 (fig. S3A-B) in cortex and different parts of hippocampus of Tg mice as compared to age-matched non-Tg mice. We also found increased Iba-1 immunoreactivity and colocalization of many Iba-1-positive cells with TLR2 (fig. S2B) and MyD88 (fig. S3B) in the cortex and hippocampus of Tg mice. Western blot experiments also confirmed the increase in TLR2 (fig. S2C-D) and MyD88 (fig. S3C-D) in the hippocampus of Tg mice as compared to non-Tg mice.

Designing of a peptide corresponding to the TLR2-interacting domain of Myd88 (TIDM) for specific targeting of TLR2: Since there is no specific inhibitor of TLR2, for the therapeutic purpose, we attempted to target TLR2. After ligand binding, TLR2 functions through MyD88 (14, 15). Therefore, we applied rigid-body protein-protein interaction tool to model the interaction between TLR-interacting domain (TIR) of TLR2 and MyD88. Since the crystal structures of TIRs of mouse TLRs were not available, we adopted *in silico* homology modeling strategy to build 3D structures of TIRs from all different TLRs (fig. S4A-G). Similar to previous finding (20), the docked pose of MyD88 and TIR complex as derived from our *in silico* modeling analyses revealed that the BB loop of TLR2 was engaged with the CD loop of MyD88 with a strong van der Waals (VDW) interaction (Fig. 2A). Therefore, we designed the following peptide corresponding to the TLR2-interacting domain of MyD88 (TIDM) from the CD loop to disrupt the interaction between TLR2 and MyD88:

Wild type (wt) TIDM: drqikiwfqnrrmkwkk^{245}PG<u>A</u>HQ<u>K</u>^{250}

Mutated (m) TIDM: drqikiwfqnrrmkwkk^{245}PG<u>W</u>HQ<u>D</u>^{250}

We added the Antennapedia homeodomain (lowercase) at the C-terminal of these peptides to facilitate cell permeability. MyD88 segments are in uppercase, and positions of mutations are underlined. Interestingly, when the interaction between TIR of TLR2 and MyD88 was modeled with wtTIDM peptide, we observed that MyD88 was associated with a certain degree of rotation, leaving its CD loop far removed from the TLR2 BB loop (Fig. 2B). According to Pydock analysis, wtTIDM peptide was found to be docked in the interface of CD loop, αB helix and BB loop of TIR domain of TLR2 (fig. S5A). That specific pose of wtTIDM peptide imposed its VDW surface to be distributed over the BB loop of TLR2 (fig. S5A), which was not possible in case of mTIDM peptide (fig. S5B). We observed that there was a strong electrostatic interaction (2.31 A°) between NE1 atom of conserved histidine residue (H82) of CD loop and ND atom of histidine (H4) residue of wtTIDM peptide (fig. S5C). The docked structures of mTIDM with

TLR2 clearly indicated that there was a very weak electrostatic interaction (7.26 A°) between H82 residue of CD loop and H4 residue of mTIDM peptide (fig. S5C; right panel). Moreover, mutation of wtTIDM from lysine to aspartate imposed a negative cloud, which also drove the C-terminal end of the mTIDM even further away from the BB loop and more towards the groove of the αB helix (fig. S5B). We also measured the possibility of VDW interaction in that complex by measuring the distance of VDW droplets between two close residues of TLR2 and MyD88 (fig. S5D). We observed that there was a significant VDW overlap between MyD88 and TLR2 in the absence of wtTIDM. However, when complexed with wtTIDM, the BB loop of TLR2 and the CD loop of MyD88 posed far away from each other, negating any possibility of VDW interaction (fig. S5E). To compare the affinity of wtTIDM and mTIDM towards TLR2 from another angle, we performed surface plasmon resonance (SPR) analysis. We first cloned and purified the whole TLR2 protein. However, it was not stable and since the whole TLR2 protein is also not available, we prepared only the C-terminal TIR domain of TLR2 protein (cTLR2) via viral cloning strategy and purified the protein by myc affinity column (Fig. 2C). Kinetic plots (Fig. 2D-E) clearly showed that increasing doses of both wtTIDM and mTIDM displayed binding with the cTLR2. However, wtTIDM displayed much stronger affinity than mTIDM towards cTLR2 (Fig. 2D-F). According to the plot of SPR response at equilibrium versus peptide concentration (Fig. 2F), the affinity of wtTIDM (K_d = 8μM) for cTLR2 was approximately 2.5 times stronger than mTIDM (K_d= 19 μM). To further substantiate, we performed a thermal-shift assay, which revealed that 10 μM of wtTIDM peptide strongly shifted the melting curve of cTLR2 (Fig. 2G). On the other hand, very little shift was observed for mTIDM (Fig. 2H). Together, these results suggest that wtTIDM is a potent small-molecule peptide that strongly interferes with the interaction between TLR2 and MyD88.

Next, we examined if wtTIDM had similar affinity towards other TLRs. Interestingly, our *in silico* analyses revealed that wtTIDM peptide docked far from the BB loop of TLR1 (Fig. 3A),

TLR4 (Fig. 3B), TLR5 (Fig. 3C), TLR6 (Fig. 3D), TLR7 (Fig. 3E), and TLR9 (Fig. 3F), suggesting that wtTIDM specifically targets the BB loop of TLR2, but not other TLRs.

Next, we examined if wtTIDM peptide could disrupt the physical association between endogenous TLR2 and MyD88. Earlier we have delineated that fibrillar Aβ1-42 activates microglia via TLR2 (17). Here, by immunoblot analysis of MyD88 immunoprecipitates with antibodies against TLR2, we found that fibrillar Aβ1-42 treatment increased the association between TLR2 and MyD88 in microglial cells and that this interaction was inhibited by wtTIDM, but not mTIDM, peptide (Fig. 3G-H). Input showed the presence of equal amount of TLR2 and MyD88 under different treatment condition (Fig. 3G). To understand the specificity, we examined the effect of wtTIDM peptide on the interaction between TLR4 and MyD88. LPS is a prototype agonist of TLR4. LPS treatment increased the association between TLR4 and MyD88 in microglial cells (Fig. 3I-J) and in contrast to the suppression of TLR2:MyD88 interaction (Fig. 3G-H), wtTIDM peptide had no effect on the interaction between TLR4 and MyD88 (Fig. 3I-J). Next, we examined if wtTIDM could interfere with the interaction between MyD88 and newly-formed Myc-tagged C-terminal TLR2 (cTLR2). Therefore, microglial cells were transduced with *pLenti-cMyc-cTlr2* lentivirions and after 48 h of transduction, cells were treated with fibrillar Aβ1-42 in the presence or absence of wtTIDM/mTIDM for 1 h. Immunoblot analysis of MyD88 immunoprecipitates with antibodies against c-Myc showed that the interaction between newly-formed cTLR2 and MyD88 in Aβ1-42-treated microglial cells was inhibited by wtTIDM, but not mTIDM, peptide (Fig. 3K-L).

TIDM peptide inhibits microglial inflammation induced by fibrillar Aβ1-42 and lipoteichoic acid (LTA), but not 1-methyl-4-phenylpyridinium (MPP^+), double-stranded RNA (poly IC), bacterial lipopolysaccharide (LPS), flagellin, and CpG DNA: Microglia expressing different TLRs are activated under various pathological conditions, such as neurodegeneration, inflammation, viral and bacterial infection, etc. (7, 21). Therefore, we investigated if TIDM

peptide was capable of suppressing microglial activation induced by different stimuli. Microglial cells pretreated with different concentrations of wtTIDM and mTIDM peptides for 1 h were stimulated with fibrillar Aβ1-42 (an etiological reagent of AD), MPP^+ (a Parkinsonian toxin), LTA (agonist of TLR2), poly IC (agonist of TLR3), LPS (agonist of TLR4), flagellin (agonist of TLR5), and CpG DNA (agonist of TLR9). As expected, fibrillar Aβ (Fig. 4A), MPP^+ (Fig. 4D), LTA (Fig. 4G), poly IC (fig. S7A), LPS (Fig. 4J), flagellin (Fig. 4M), and CpG DNA (Fig. 4P) induced the activation of NF-κB in microglial cells. However, wtTIDM peptides inhibited fibrillar Aβ- and LTA-mediated activation of NF-κB (Fig. 4A & 4G). In contrast, wtTIDM peptides remained unable to suppress the activation of NF-κB in microglial cells induced by MPP^+ (Fig. 4D), poly IC (fig. S7A), LPS (Fig. 4J), flagellin (Fig. 4M), and CpG DNA (Fig. 4P). These results were specific as mTIDM peptides had no effect on the activation of NF-κB induced by any of the stimuli. Activation of classical NF-κB pathway involves the phosphorylation of IκBα followed by nuclear translocation of p65 and p50. Therefore, we also investigated the effect of wtTIDM peptide on nuclear translocation of p65 and p50 in activated microglia. As expected, increased nuclear translocation of p65 and p50 was observed in microglial cells in response to fibrillar Aβ1-42 (fig. S8A-C) and LPS (fig. S8D-F). However, wtTIDM peptide treatment inhibited nuclear translocation of p65 and p50 in microglial cells stimulated with fibrillar Aβ1-42 (fig. S8A-C), but not LPS (fig. S8D-F), indicating the specificity of wtTIDM peptide. To confirm these results, we also monitored the expression of IL-1β and iNOS, proinflammatory molecules that are driven by NF-κB activation. All the stimuli induced the expression of IL-1β and iNOS in microglial cells (Fig. 4B-C, 4E-F, 4H-I, 4K-L, 4N-O, 4Q-R, fig. S6A-F, & fig. S7B-D). Consistent to the effect of wtTIDM on NF-κB activation, wtTIDM peptides inhibited the expression of proinflammatory molecules induced only by fibrillar Aβ (fig. S6A & Fig. 4B-C) and LTA (fig. S6C & Fig. 4H-I), but not MPP^+ (fig. S6B & Fig. 4E-F), poly IC (fig. S7B-D), LPS (fig. S6D & Fig. 4K-L), flagellin (fig. S6E & Fig. 4N-O), and CpG DNA

(fig. S6F & Fig. 4Q-R). These results suggest that wtTIDM peptide specifically inhibits microglial inflammation induced by agonists of TLR2, but not other TLRs.

The wtTIDM peptide does not inhibit fibrillar Aβ1-42-induced activation of microglia in the absence of TLR2: Since wtTIDM peptide disrupted the physical association between TLR2 and MyD88, as a mechanistic proof-of-principal, we examined the effect of wtTIDM peptide on Aβ1-42-induced activation of *Tlr2*$^{-/-}$ microglia. Similar to BV-2 microglial cells, fibrillar Aβ1-42 peptides strongly induced the activation of NF-κB in primary microglia isolated from WT mice, which was inhibited by wtTIDM peptide (fig. S9A). On the other hand, fibrillar Aβ1-42 peptides weakly induced the DNA-binding activity of NF-κB in *Tlr2*$^{-/-}$ microglia (fig. S9A). However, in contrast to WT microglia, wtTIDM peptide remained unable to inhibit fibrillar Aβ1-42-induced activation of NF-κB in *Tlr2*$^{-/-}$ microglia (fig. S9A-B). To further confirm, we also measured levels of common proinflammatory cytokines (TNFα and IL-1β) in supernatants. Similar to NF-κB activation, the induction of TNFα and IL-1β production by fibrillar Aβ1-42 was low in *Tlr2*$^{-/-}$ microglia as compared to WT microglia (fig. S9C-F). However, wtTIDM peptide inhibited fibrillar Aβ1-42 peptide-induced production of TNFα and IL-1β in WT, but not *Tlr2*$^{-/-}$, microglia (fig. S9C-F), suggesting that wtTIDM peptide needs TLR2 to exhibit its function.

Intranasal administration of wtTIDM peptide inhibits inflammation, reduces plaque load and decreases hyperphosphorylation of tau in the hippocampus of 5XFAD Tg mice: It is becoming clear that glial inflammation plays an important role in the loss of neurons in AD and other neurodegenerative disorders (7, 9, 22-24). Since wtTIDM peptide specifically inhibited fibrillar Aβ1-42-mediated microglial activation, we decided to test its therapeutic translatability in 5XFAD Tg mice. We first determined whether wtTIDM peptide could enter into the hippocampus. Tg mice were treated with TIDM peptides intranasally and after 60 min of administration, we detected wtTIDM peptide in the hippocampus of Tg mice by electrospray ionization-coupled mass spectrometry (Fig. 5A & C). In contrast, the hippocampus of saline-

treated Tg mice did not exhibit any peak for wtTIDM peptide (Fig. 5B). The level of wtTIDM peptide was 23.33 ±14.14 ng per gram brain tissue in the hippocampus of wtTIDM-treated Tg mice in comparison with nil in saline-treated Tg mice. By infrared scanning, we also detected TIDM peptide in hippocampus after intranasal treatment (fig. S10). Therefore, after intranasal administration, TIDM peptide enters into the hippocampus.

Next, we investigated whether intranasal TIDM peptide was capable of modulating NF-κB activation in the hippocampus of Tg mice. As seen by double-label immunofluorescence of hippocampal sections, levels of Iba-1 and phospho-p65 were markedly higher in Tg mice as compared to non-Tg mice (Fig. 5D-H). However, intranasal treatment of Tg mice with wtTIDM, but not mTIDM, peptides led to the suppression of both Iba-1 and phospho-p65 in the hippocampus of Tg mice (Fig. 5D-H). This was also confirmed by Western blot analysis of hippocampal tissues (fig. S11A-B). Moreover, activated microglia are known to express iNOS (21, 25). Accordingly, hippocampal microglia of Tg mice were also positive for iNOS (fig. S12 & Fig. 5I-J). However, wtTIDM, but not mTIDM, peptide suppressed the expression of iNOS in the hippocampus of Tg mice (fig. S12 & Fig. 5I-J). Western blot analysis also confirms inhibition of hippocampal iNOS expression by wtTIDM, but not mTIDM, peptide treatment (Fig. 5K-L).

Amyloid plaque is an important feature of AD pathology, which is modeled in 5XFAD Tg mice (26, 27). Therefore, next, we examined if wtTIDM treatment was capable of reducing the load of amyloid plaques from the hippocampus of Tg mice. Immunostaining of hippocampal sections with 82E1 mAb (Fig. 5M-O) as well as Western blot analysis of hippocampal tissues with 6E10 mAb (Fig. 5P-Q) and 82E1 mAb (fig. S13A-B) showed markedly higher level of Aβ peptides in the hippocampus of Tg mice as compared to non-Tg mice. Similarly, ELISA of serum (fig. S14A-B), TBS-extracted hippocampal fractions (fig. S14C-D) and (TBS+Triton X-100)-extracted hippocampal fractions (fig. S14E-F) also demonstrated marked increase in Aβ1-40 and

Aβ1-42 in Tg mice as compared to non-Tg mice. However, a significant decrease in Aβ was seen with wtTIDM, but not mTIDM, treatment (fig. S13A-B, fig. S14A-F & Fig. 5M-Q). These results suggest that intranasal administration of wtTIDM is capable of reducing Aβ burden in the hippocampus of 5XFAD mice.

Hyperphosphorylation of tau is another prominent feature of AD pathology (28, 29). It has been shown that hyperphosphorylation at Ser396 of tau occurs in the hippocampus of 5XFAD mice at a much earlier stage than the appearance of learning and memory impairment (30). Therefore, we examined the effect of TIDM peptide treatment on the status of tau phosphorylation *in vivo* in the hippocampus of Tg mice. Immunoblot analysis indicates a marked increase in phospho-tau in hippocampal extracts of Tg mice as compared to non-Tg mice (fig. S15A-B). However, treatment of Tg mice with wtTIDM, but not mTIDM, peptide led to the suppression of phospho-tau in the hippocampus without affecting the total level of tau protein (fig. S15A-B), indicating that wtTIDM peptide treatment is adequate in decreasing tau phosphorylation in the hippocampus of Tg mice.

Reduction in neuronal apoptosis and protection of memory and learning in 5XFAD Tg mice by intranasal administration of wtTIDM peptide: Since neuroinflammation may be associated with neuronal apoptosis, next, we examined if wtTIDM peptide treatment was able to reduce neuronal apoptosis in the hippocampus of Tg mice. A number of TUNEL-positive bodies co-localized with NeuN in the hippocampus of Tg mice as compared to non-Tg mice (Fig. 6A-C). However, wtTIDM, but not mTIDM, peptide attenuated neuronal apoptosis in the hippocampus (Fig. 6A-C). This result was confirmed by detection of cleaved caspase 3. As expected, the level of cleaved caspase 3 increased in the hippocampus of Tg mice (Fig. 6D-E). However, treatment of Tg mice with wtTIDM, but not mTIDM, peptide reduced the elevated level of cleaved caspase 3 in the hippocampus (Fig. 6D-E), suggesting that wtTIDM peptide treatment is capable of decreasing neuronal apoptosis *in vivo* in the hippocampus of Tg mice. Accordingly, levels of plasticity-related molecules (PSD-95, NR2A and GluR1) decreased in the hippocampus of Tg

mice as compared to non-Tg mice (Fig. 6F-I). However, consistent to the suppression of neuronal apoptosis, treatment of Tg mice with wtTIDM, but not mTIDM, peptide led to significant restoration of PSD-95, NR2A and GluR1 proteins *in vivo* in the hippocampus (Fig. 6F-I).

The ultimate objective of neuroprotection in AD is to improve and/or protect memory. Major functions of the hippocampus are to generate and organize long-term memory and spatial learning. Therefore, we examined if wtTIDM peptide protected memory and learning in Tg mice. As expected, Tg mice took much longer time to find the food reward hole and exhibited a greater latency [$p<0.001(=0.0000213)$] with higher errors [$p<0.001(=0.0000251)$ in the Barnes maze as compared to non-Tg mice. However, wtTIDM treatment significantly improved the memory functions of Tg mice as shown by latency [$F3,28=93.153$, $p<0.001(=0.0000112)$] (Fig. 6J) and number of errors [$F3,28=36.339$, $p<001(=0.0000863)$] (Fig. 6K). Memory functions of wtTIDM peptide-treated mice were also better in locating the reward hole with less latency [$p<0.001(=0.0000600)$] and fewer errors [$p<0.001(=0.0000579)$] when compared to mTIDM treated mice. Similarly, on T maze, untreated Tg mice also exhibited fewer number of positive turns [$p<0.001(=0.0000440)$] and higher number of negative turns [$p<0.001(=0.000223)$] than age-matched non-Tg mice (Fig. 6L-M). However, wtTIDM treatment displayed significant effect on successful positive turns [$F3,28=31.475$, $p<0.001(=0.0000411$] (Fig. 6L) and also lesser number of errors [$F3,28=26.653$, $p<0.001(=0.0000235$] (Fig. 6M) by Tg mice. Again, wtTIDM-treated mice exhibited a greater number of positive turns [$p<0.001(=0.0000954)$] and less negative turns [$p<0.001(=0.000123)$] as compared to mTIDM-treated Tg mice (Fig. 6L-M). We also monitored short-term memory of Tg mice by Novel Object Recognition (NOR) test. Tg mice exhibited significant deficits [$p<0.001(=0.0000149)$] in NOR test evidenced by discrimination index (Fig. 6N) compared to age-matched non-Tg mice. However, wtTIDM peptide-treated mice showed significant improvement ($p<0.001$) in short-term memory as compared to either untreated Tg or mTIDM-treated Tg mice (Fig. 6N). On the other hand, gross

motor activities of Tg and non-Tg mice were almost similar (fig. S16). Furthermore, either wtTIDM or mTIDM peptide did not modulate gross motor activities in Tg mice as evident from number of movements, horizontal activity, rest time, and stereotypy (fig. S16A-D), suggesting that improvement of memory by wtTIDM peptide treatment is not due to any alteration in gross motor activities.

The wtTIDM peptide requires TLR2 to reduce plaques and improve memory in 5XFAD Tg mice: To confirm that wtTIDM peptide in fact requires TLR2 to exhibit its function *in vivo*, we crossed *Tlr2*$^{-/-}$ mice with Tg mice to create 5XFAD mice null for *Tlr2* (Tg-*Tlr2*$^{-/-}$). The *Tlr2* knockdown did not alter insertion or expression of the 5XFAD transgenes, and vice versa (fig. S17*A*). Six month old WT, *Tlr2*$^{-/-}$, Tg, and Tg-*Tlr2*$^{-/-}$ mice did not differ significantly with respect to gross body weight or wet brain weight (fig. S17*B*-*C*). We also did not find any overt phenotypic differences, including diet, fecal boli, social interaction, and agitation across genotypes at this age. Although wtTIDM peptide reduced plaque load and improved spatial learning and memory in Tg mice (Figs. 5-6), it remained unable to do so in Tg-*Tlr2*$^{-/-}$ mice (fig. S17D-G), indicating that wtTIDM peptide is ineffective in the absence of *Tlr2*.

The wtTIDM, but not mTIDM, peptide suppresses the disease process of experimental allergic encephalomyelitis (EAE) and collagen-induced arthritis (CIA) in mice: Being an important member of the innate immune pathways, Myd88-dependent TLR2 signaling plays an important role in the pathogenesis of a wide variety of infectious and autoimmune disorders (31, 32). Therefore, we examined whether the function of wtTIDM peptide was limited to only 5XFAD mice or other disease models as well. EAE is the widely-used animal model of multiple sclerosis (MS) and chronic form of EAE is modeled in male C57/BL6 mice upon immunization with MOG35-55. Similar to its effect in 5XFAD mice, intranasal treatment of EAE mice with wtTIDM peptide strongly inhibited the clinical symptoms of EAE (Fig. 7A). While comparing the means between groups with Dunnett's multiple comparison analyses, we found that there was

significant difference of means between EAE and EAE+*wt*TIDM (adjusted $p<0.001$). On the other hand, mTIDM peptide had no effect (Fig. 7A), suggesting the specificity of the effect. As expected, induction of EAE reduced locomotor activities in mice that are evident by heat-map analysis (Fig. 7B), distance traveled (Fig. 7C), rearing (Fig. 7D), velocity (Fig. 7E), and acceleration (Fig. 7F). Footprint analysis (fig. S18) also indicated decrease in stride length (Fig. 7G) and point length (Fig. 7H) and increase in sway length (Fig. 7I) and toe spread (Fig. 7J) in EAE mice as compared to normal mice. We also found dragging of toes frequently in EAE mice (fig. S18). However, intranasal treatment by wtTIDM, but not mTIDM, peptide improved locomotor activities and normalized footprints in EAE mice (Fig. 7A-K & fig. S18). CIA is a widely-used animal model of rheumatoid arthritis. Similar to EAE mice, wtTIDM, but not mTIDM, peptide also decreased clinical symptoms of CIA in mice (Fig. 7L). While comparing the means between groups with Dunnett's multiple comparison analyses, we found that there was significant difference of means between CIA and CIA+*wt*TIDM [adjusted $p = 0.0148 (<0.05)$]. The wtTIDM peptide also enhanced locomotor activities (Fig. 7N-R), and improved footprint behavior (Fig. 7S-V & fig. S19).

Discussion

Deciphering the mechanism of the disease process of AD and developing an effective neuroprotective therapeutic approach to slow down or halt the disease progression are of paramount importance. TLRs are known to resolve innate immune response by perceiving pathogen-associated molecular patterns and endogenous damage-associated molecular patterns (15). Microglia in the CNS express most of the TLRs known to date and earlier we have shown that out of different TLRs, fibrillar Aβ1-42 requires TLR2 to stimulate microglial inflammation (17). Accordingly, several studies have extended this finding either by demonstrating a direct interaction between TLR2 and Aβ or via CD14 (18, 19, 33). Here, we describe an important role

of TLR2 in Alzheimer's disease. We detected higher levels of TLR2 in hippocampus and prefrontal cortex of persons with AD dementia compared to persons with MCI or NCI. Although some studies reported the involvement of TLR4 in Aβ-mediated microglial activation, we did not find higher levels of TLR4 in the CNS of persons with AD dementia indicating the specificity of our finding. *Tlr2* polymorphism has been reported to influence the susceptibility of AD (34) and PBMC of AD patients also express increased level of TLR2 (35). Consistent to TLR2, we also observed upregulation of MyD88 in the CNS of persons with AD dementia and interestingly, both TLR2 and MyD88 positively correlated with Braak score. MyD88 also correlated negatively with cognitive function.

Although TLR2 is an important member of innate immunity, there was no specific inhibitor for targeting TLR2. Therefore, through structural analysis of the interaction between TLR2 and MyD88, we have designed a peptide corresponding to the TLR2-interacting domain of MyD88 (TIDM) from the CD loop. Since the BB loop of TLR2 interacts with the CD loop of MyD88, wtTIDM peptide disrupts the association between TLR2 and MyD88. Interestingly, wtTIDM peptide docks in a way that it specifically targets the BB loop of TLR2, but not other TLRs, thereby inhibiting signaling pathways transduced by TLR2 only. Since wtTIDM peptide specifically targets TLR2 and fibrillar Aβ1-42 requires TLR2 for microglial activation (17, 18), wtTIDM peptide inhibits microglial NF-κB activation and inflammation induced by only LTA (a known agonist of TLR2) and fibrillar Aβ1-42, but not by MPP^+, poly IC (an agonist of TLR3), LPS (an agonist of TLR4), flagellin (an agonist of TLR5), and CpG DNA (an agonist of TLR9), indicating the selective inhibition of TLR2 pathway by wtTIDM peptide. Moreover, consistent to the disruption of TLR2:MyD88 interaction, wtTIDM peptide does not function in the absence of TLR2.

Unmodified peptides usually have short half-lives due to rapid proteolysis in blood, kidneys, or liver and/or accelerated renal clearance, which are the major challenges of most peptide therapy.

However, it has been shown that Drosophila antennapedia homeodomain-derived cell-penetrating peptide, penetratin, being rich in positively charged residues, helps cargo peptides to translocate into the cells, therefore avoiding rapid proteolysis (36, 37). Moreover, unmodified peptides do not enter into the CNS and we have seen that penetratin can breach the tight endothelial network and carry peptides across the BBB (23, 38). Therefore, we tested the efficacy of penetratin-containing wtTIDM peptide in Tg mice and demonstrated that wtTIDM peptide reduced microglial inflammation, decreased neuronal apoptosis and protected cognitive function from AD toxicity. Our conclusions are based on the following. *First*, after intranasal administration, TIDM peptide entered into the hippocampus. *Second,* wtTIDM, but not mTIDM, peptide inhibited hippocampal activation of NF-κB and microglial inflammation in Tg mice. *Third,* wtTIDM, but not mTIDM, peptide protected hippocampal neurons and NMDA and AMPA receptor proteins from Alzheimer's toxicity in Tg mice. *Fourth,* wtTIDM, but not mTIDM, peptide also improved spatial learning and memory in Tg mice. Furthermore, we did not notice any drug-related side effect (e.g. hair loss, appetite loss, weight loss, untoward infection, etc.) in any of the TIDM-treated mice used during the course of the study. However, one study has shown that genetic knockdown of TLR2 accelerates the cognitive decline in APP Tg mice (39). It is definitely possible as complete knockdown of TLR2 wipes out basal as well as induced TLR2 signaling pathways. Moreover, TLR2 has been shown to function via both MyD88-dependent and -independent pathways (40, 41) and the beauty of our finding is that TIDM peptide targets only the MyD88-dependent induced TLR2 signaling pathway without inhibiting basal TLR2 activity.

Whether plaques are directly related to the loss of memory in AD or not, amyloid plaque is one of the pathological hallmarks in AD and it is also important to see that wtTIDM, but not mTIDM, peptide treatment reduced hippocampal plaque load in Tg mice. However, at present, we do not know how wtTIDM peptide treatment is coupled to plaque reduction. Beta-secretase 1

(BACE1) is the key enzyme that initiates the formation of Aβ and it has been shown that inhibition of NF-κB prevents Aβ-induced BACE1 promoter transactivation and that overexpression of wild-type or Swedish mutated βAPP does not modify the transactivation of BACE1 promoter constructs lacking NF-κB-responsive element (42). Since wtTIDM peptide suppresses fibrillar Aβ-induced activation of NF-κB, it is possible that wtTIDM peptide reduces the plaque burden in Tg mice via attenuation of the NF-κB-BACE1 pathway.

There is no effective therapy for halting the progression of AD. Administration of different inhibitors of cholinesterase such as Aricept®, Exelon®, Razadyne®, Cognex® etc. has been the standard treatment for AD (43). However, it is often associated with a number of side effects and unsatisfactory outcomes. Here, we have demonstrated that levels of TLR2 and MyD88 are upregulated in the CNS of AD patients, that TLR2 and MyD88 positively correlate with Braak score, that wtTIDM peptide targets only TLR2 without modulating other signaling pathways, and that after intranasal administration, wtTIDM peptide reaches the hippocampus, suppresses hippocampal NF-κB activation, inhibits microglial inflammation, lowers cerebral plaque load, attenuates neuronal apoptosis, and protects learning and memory in Tg mice. These results suggest that selective targeting of TLR2 by intranasal wtTIDM peptide may have therapeutic importance in AD. Moreover, wtTIDM peptide also improved functional impairment and suppressed disease processes of EAE and CIA in mice. Therefore, in addition to AD, TIDM peptide may also open up an opportunity for a number of other disorders.

Materials and methods

Human Subjects

Thirty-three cases with antemortem clinical diagnosis of no cognitive impairment (NCI; n=12), mild cognitive impairment (MCI; n=11), and AD (n=10) obtained from the Rush Religious Order Study (RROS) (44, 45) were analyzed (table S1). All participants agreed to a detailed annual clinical evaluation and brain donation upon death.

Clinical and Neuropathologic Evaluations

Clinical criteria for diagnosis of NCI, MCI and AD have been reported elsewhere (44, 46). Final clinical and neuropsychological testing, which included the Mini-Mental State Examination (MMSE) and a battery of 19 cognitive tests, was performed within 2 years prior to death. A global cognitive *z* score (GCS) comprising the 19 tests was available for all cases (47). Braak staging of neurofibrillary tangles (NFTs) (48) was performed as previously described (44). Subjects with pathological findings other than AD (e.g. stroke, Parkinson disease, Lewy body dementia) were excluded from the study. Tissue and clinical information is under the protection of the Health Information Privacy Administration rules.

Tissue Samples and Western Blotting

Superior frontal cortex (Brodmann area 9) was dissected free of white matter at autopsy on dry ice to prevent thawing and was maintained at −80°C until assay. Tissue was homogenized and processed as described earlier (22). Tissue extracts and cell lysates (30μg) were electrophoresed on 8 or 10% Bis-Tris SDS polyacrylamide gels in a continuous buffer system, transferred to nitrocellulose membranes (BioRad) with a semi-dry blotter (Pierce) and immunoblotted as described earlier (22, 49-51). Blots were converted to binary, analyzed using ImageJ (NIH) and normalized to loading control (β-actin).

Preparation of C-terminal TLR2 (cTLR2)

TLR2 full-length construct (*pLenti-cmyc-DDK/ tlr2)* was purchased from Origene. The cTLR2 (640-784 amino acids) tagged with c-myc was cloned in lenti vector using TOPO TA cloning kit (K5310-00; Life technologies). Briefly, a kozak sequence was incorporated in the upstream of C-terminal TIR domain of TLR2. Next, cTLR2 was cloned in lentivector followed by packaging in lentivirus using HEK293FT cells. After 48h, media was collected and concentrated with Lenti-X Concentrator (Cat# 631231; Clontech). This concentrated lentiviral sup was used for viral transduction. The cTLR2 protein was isolated from HEK293 cell lysate by passing through Myc affinity column. Purified protein was desalted and concentrated by using 10 kD molecular cut-off filtration system.

Surface Plasmon Resonance

To analyze the binding of TLR2 with TIDM peptides, surface plasmon resonance (SPR) experiments were carried out using a Reichert 4SPR instrument (Reichert Technologies, Buffalo, NY). Binding assay was performed using a 500 kDa Carboxymethyl Dextran Gold Sensor Slide (Reichert Inc.) for capturing TLR2. Protein immobilization was at a flow rate of 30 µl/min in PBS for 3 min with 0.8 mg/mL solution of TLR2. For analyte association, different concentrations of wtTIDM and mTIDM peptides in PBS running buffer were injected for 2.5 min at a rate of 30 µl/min followed by a dissociation phase of 3 min. The sensor surface was regenerated after each dissociation cycle by allowing buffer to flow at 40 µl/min for a minimum of 15 min. Signals obtained for the TLR2-bound surface were subtracted by signals obtained for the reference cell according to standard procedure using the system software. The concentration dependence of the subtracted signal was analyzed to determine binding affinity of TLR2 with wtTIDM and mTIDM peptides.

Thermal shift assays

Thermal shift assays were performed in an Applied Biosystems 7500 standard real-time thermal cycler machine as described before (52, 53). For each reaction, purified protein (0.5 µg to 1µg) was added to 18 µL of thermal shift buffer provided with the kit, and 1- 2µL of dye. Reaction was set 96 well PCR plate in the dark and then placed in the thermal cycler machine using the following two-stage program [(25°C for 2 mins) 1 cycle; (27°C for 15 sec, 26 °C for 1 min) 70 cycles; auto increment 1°C for both stages]. The filter was set at ROX with no quencher filter and no passive filter.

In silico structural analysis

We utilized Deep View 3.7β2, an online macromolecular analytical tool of Expert Protein Analytical System (ExPASy), to model structures of TIR domains of different TLRs (TLR1, TLR2, TLR4, TLR5, TLR6, TLR7, and TLR9). In order to evaluate the quality of modeled structures, we used Quality Measurement Analysys tool (QMEAN), a composite scoring tool that estimates the global quality of the entire model as well as the local per-residue analysis of

different regions within a model. Residue-level interaction was evaluated by Cβ atom potential and long-range interactions were validated by all-atom potential. A solvation potential was implemented to analyze the burial status of the residues. The local geometry of each structure was analyzed by a torsion angle potential over three consecutive amino acids. The docked pose of TIR domains with either wtTIDM or mTIDM peptide was derived from pydock rigid-body protein-protein docking tool.

Animals and Intranasal Delivery of TIDM Peptides

B6SJL-Tg(APPSwFlLon,PSEN1*M146L*L286V)6799Vas/J transgenic (5XFAD or termed here as Tg) mice were purchased from Jackson Laboratories (Bar Harbor, ME). Six-month old male Tg mice were treated intranasally with wtTIDM or mTIDM peptides (0.1 mg/Kg body wt/2d) for 30d. Briefly, TIDM peptides were dissolved in 5 µl normal saline, mice were hold in supine position and saline was delivered into one nostril using a pipetman.

Induction of chronic EAE and treatment by TIDM peptides

Male C57BL/6 mice were immunized with 100 µg of MOG35-55 as described by us (54, 55). Mice also received two doses of pertussis toxin (150 ng/mouse) on 0 and 2 day post-immunization (dpi). Starting from 10 dpi, mice received wtTIDM or mTIDM peptides (0.1 mg/Kg body wt/d) intranasally.

Induction of collagen-induced arthritis (CIA) and treatment by TIDM peptides

Male DBA/1J mice (8-9 week old) were immunized intradermally at the base of the tail with 100 µg of bovine type II collagen emulsified in Incomplete Freund's Adjuvant and *M. tuberculosis* H37RA. On 21 dpi, mice were boosted with an intraperitoneal injection of 100 µg of bovine type II collagen. Mice were treated wtTIDM or mTIDM peptides (1 mg/Kg body wt/d) i.p. starting from 29 dpi.

Preparation of fibrillar Aβ1-42

Fibrillar Aβ1-42 (Anaspec, Fremont, CA) were prepared by incubating freshly solubilized peptides at 50 μM in sterile distilled water at 37 °C for 5 days (56). Please see figure S20 for morphology of fibrillar Aβ1-42.

Semi-quantitative RT-PCR analysis: Total RNA was isolated from hippocampus using Ultraspec-II RNA reagent (Biotecx Laboratories, Inc., Houston, TX) following the manufacturer's protocol. To remove any contaminating genomic DNA, total RNA was digested with DNase. RT-PCR was carried out as described earlier (23, 57) using a RT-PCR kit (Clontech, Mountain View, CA).

Real-time PCR analysis: DNase-digested RNA was analyzed by real-time PCR in the ABI-Prism7700 sequence detection system (Applied Biosystems, Foster City, CA) as described earlier (23, 57).

Electrophoretic Mobility Shift Assay (EMSA): Nuclear extracts were isolated and EMSA was carried out as described before (22, 23).

Barnes Maze and T Maze: Maze experiments were performed as described by us (52, 57). Briefly, for Barnes maze, mice were trained for 2 consecutive days followed by examination on day 3. After each training session, maze and escape tunnel were thoroughly cleaned with a mild detergent to avoid instinctive odor avoidance due to mouse's odor from the familiar object. On day 3, the maze was illuminated with high wattage light that generated enough light and heat to motivate animals to enter into the escape tunnel, allowing us to measure latency (duration before all four paws were on the floor of the escape box) and errors (incorrect responses before all four paws were on the floor of the escape box).

For T-maze, mice were also habituated in the T-maze for two days under food-deprived conditions so that animals can eat food rewards at least five times during 10 minutes period of training. During each trial, mice were placed in the start point for 30 s and then forced to make a right arm turn which was always baited with color food chips. After each training session, T maze was thoroughly cleaned with a mild detergent. On day 3, mice were tested for making

positive turns and negative turns. The reward side is always associated with a visual cue. Number of times the animal eats the food reward would be considered as a positive turn.

Novel Object Recognition Task: Novel object recognition task was performed to monitor the short term memory as described by others (58) and us (57). Briefly, during training, mice were placed in a square novel box (20 inches long by 8 inches high) surrounded with infrared sensor. Two plastic toys (between 2.5 and 3 inches) that varied in color, shape, and texture were placed in specific locations in the environment 18 inches away from each other. The mice were able to explore freely the environment and objects for 15 min and then were placed back into their individual home cages. After 30 mins, mice were placed back into the environment with two objects in the same locations, but now one of the familiar objects was replaced with a third novel object. The mice were then again allowed to explore freely both objects for 15 min. The objects were thoroughly cleaned with a mild detergent.

Immunohistochemistry: Mice were anesthetized with ketamine-xylazine injectables and perfused with PBS and then with 4% (w/v) paraformaldehyde in PBS followed by dissection of the brain from each mouse for immunofluorescence microscopy (23, 59). Briefly, samples were incubated in PBS containing 0.05% Tween 20 (PBST) and 10% sucrose for 3 h and then 30% sucrose overnight at 4 °C. Brain was then embedded in O.C.T (Tissue Tech) at -80 °C, and processed for conventional cryosectioning. Frozen sections (30 μm) were treated with cold ethanol (-20 °C) followed by two rinses in PBS, blocking with 3% BSA in PBST and double-labeling with two antibodies (table S3). After three washes in PBST, sections were further incubated with Cy2 and Cy5 (Jackson ImmunoResearch Laboratories, Inc.). The samples were mounted and observed under an Olympus IX81 fluorescence microscope. Counting analysis was performed using Olympus Microsuite V software with the help of touch counting module.

Fragment End Labeling of DNA: It was performed using a commercially available kit (TdT FragEL^{TM}, Calbiochem) as described before (10, 22).

ELISA for $A\beta_{1-42}$ and $A\beta_{1-40}$: Hippocampal tissues were homogenized in TBS, pelleted for 30 min × 150,000 *g*. The pellet was resuspended in 3 volumes (wt/vol original tissue weight) of TBS+1% Triton X-100, pelleted for 30 min × 150,000 *g* and the supernatant recovered and stored. Samples were assayed for protein concentration and diluted 10-fold prior to performing ELISA according to manufacturer's instruction (BioLegend).

Statistical Analysis: Clinical and biochemical data of human tissues were compared across diagnoses using nonparametric tests (i.e., Kruskal-Wallis test or Fisher's exact test, with Dunn's correction for multiple comparisons), which are more robust to outliers, non-normality and unequal sample sizes. Two-tailed Spearman Rank-Order correlations assessed variable associations between cognitive test scores and protein optical densities. Correlations were unadjusted for demographic information (i.e., age, sex, etc.) as these metrics were not significantly different between clinical groups. Statistical tests were performed using SPSS 19 (IBM), and significance was set at $\alpha = .05$ (two-sided).

Mouse behavioral measures were examined by an independent one-way ANOVA using SPSS. Homogeneity of variance between test groups was examined using Levene's test. *Post-hoc* analyses were conducted using Tukey's or Games-Howell tests, where appropriate. Other data were expressed as means ± SD of three independent experiments. Statistical differences between means were calculated by the Student's *t*-test (two-tailed). A *p*- value of less than 0.05 ($p<0.05$) was considered statistically significant.

Study approval: Human Investigations Committees of the Rush University Medical Center approved the RROS study. Animals were maintained, and experiments were conducted in accordance with National Institutes of Health guidelines and were approved by the Rush University Medical Center Institutional Animal Care and Use Committee.

Acknowledgements

This study was supported by grants from U.S. Army Medical Research and Materiel Command (W81XWH-12-1-0065) and NIH (AG050431), the Zenith Fellows Award (ZEN-17-438829) from Alzheimer's Association, and a merit award (1I01BX003033) from US Department of Veterans Affairs.

Author contributions:

SBR, AR, MJ, and GTC designed and performed experiments; MK, SC, SM, SD, RKM, and CHL performed experiments; EJM and DAB provided reagents and wrote the manuscript; KP designed the project and wrote the manuscript.

References

1. Tanzi RE, and Bertram L. Twenty years of the Alzheimer's disease amyloid hypothesis: a genetic perspective. *Cell.* 2005;120(4):545-55.
2. Hardy J, Duff K, Hardy KG, Perez-Tur J, and Hutton M. Genetic dissection of Alzheimer's disease and related dementias: amyloid and its relationship to tau. *Nat Neurosci.* 1998;1(5):355-8.
3. Raichlen DA, and Alexander GE. Exercise, APOE genotype, and the evolution of the human lifespan. *Trends Neurosci.* 2014;37(5):247-55.
4. Rapoport M, Dawson HN, Binder LI, Vitek MP, and Ferreira A. Tau is essential to beta -amyloid-induced neurotoxicity. *Proc Natl Acad Sci U S A.* 2002;99(9):6364-9.
5. Roberson ED, Scearce-Levie K, Palop JJ, Yan F, Cheng IH, Wu T, et al. Reducing endogenous tau ameliorates amyloid beta-induced deficits in an Alzheimer's disease mouse model. *Science.* 2007;316(5825):750-4.
6. Benilova I, Karran E, and De Strooper B. The toxic Abeta oligomer and Alzheimer's disease: an emperor in need of clothes. *Nat Neurosci.* 2012;15(3):349-57.
7. Heppner FL, Ransohoff RM, and Becher B. Immune attack: the role of inflammation in Alzheimer disease. *Nat Rev Neurosci.* 2015;16(6):358-72.
8. Xu H, Gelyana E, Rajsombath M, Yang T, Li S, and Selkoe D. Environmental Enrichment Potently Prevents Microglia-Mediated Neuroinflammation by Human Amyloid beta-Protein Oligomers. *J Neurosci.* 2016;36(35):9041-56.
9. Nathan C, Calingasan N, Nezezon J, Ding A, Lucia MS, La Perle K, et al. Protection from Alzheimer's-like disease in the mouse by genetic ablation of inducible nitric oxide synthase. *J Exp Med.* 2005;202(9):1163-9.
10. Jana A, and Pahan K. Fibrillar amyloid-beta-activated human astroglia kill primary human neurons via neutral sphingomyelinase: implications for Alzheimer's disease. *J Neurosci.* 2010;30(38):12676-89.
11. Meda L, Cassatella MA, Szendrei GI, Otvos L, Jr., Baron P, Villalba M, et al. Activation of microglial cells by beta-amyloid protein and interferon-gamma. *Nature.* 1995;374(6523):647-50.

12. Mrak RE, Sheng JG, and Griffin WS. Correlation of astrocytic S100 beta expression with dystrophic neurites in amyloid plaques of Alzheimer's disease. *J Neuropathol Exp Neurol.* 1996;55(3):273-9.
13. Vlad SC, Miller DR, Kowall NW, and Felson DT. Protective effects of NSAIDs on the development of Alzheimer disease. *Neurology.* 2008;70(19):1672-7.
14. Beutler B. Inferences, questions and possibilities in Toll-like receptor signalling. *Nature.* 2004;430(6996):257-63.
15. O'Neill LA, Golenbock D, and Bowie AG. The history of Toll-like receptors - redefining innate immunity. *Nat Rev Immunol.* 2013;13(6):453-60.
16. Rivest S. Regulation of innate immune responses in the brain. *Nat Rev Immunol.* 2009;9(6):429-39.
17. Jana M, Palencia CA, and Pahan K. Fibrillar amyloid-beta peptides activate microglia via TLR2: implications for Alzheimer's disease. *J Immunol.* 2008;181(10):7254-62.
18. Liu S, Liu Y, Hao W, Wolf L, Kiliaan AJ, Penke B, et al. TLR2 is a primary receptor for Alzheimer's amyloid beta peptide to trigger neuroinflammatory activation. *J Immunol.* 2012;188(3):1098-107.
19. Reed-Geaghan EG, Reed QW, Cramer PE, and Landreth GE. Deletion of CD14 attenuates Alzheimer's disease pathology by influencing the brain's inflammatory milieu. *J Neurosci.* 2010;30(46):15369-73.
20. Gay NJ, Symmons MF, Gangloff M, and Bryant CE. Assembly and localization of Toll-like receptor signalling complexes. *Nat Rev Immunol.* 2014;14(8):546-58.
21. Gonzalez-Scarano F, and Baltuch G. Microglia as mediators of inflammatory and degenerative diseases. *Annu Rev Neurosci.* 1999;22:219-40.
22. Rangasamy SB, Corbett GT, Roy A, Modi KK, Bennett DA, Mufson EJ, et al. Intranasal Delivery of NEMO-Binding Domain Peptide Prevents Memory Loss in a Mouse Model of Alzheimer's Disease. *J Alzheimers Dis.* 2015;47(2):385-402.
23. Ghosh A, Roy A, Liu X, Kordower JH, Mufson EJ, Hartley DM, et al. Selective inhibition of NF-kappaB activation prevents dopaminergic neuronal loss in a mouse model of Parkinson's disease. *Proc Natl Acad Sci U S A.* 2007;104(47):18754-9.
24. Mondal S, Roy A, Jana A, Ghosh S, Kordower JH, and Pahan K. Testing NF-kappaB-based therapy in hemiparkinsonian monkeys. *J Neuroimmune Pharmacol.* 2012;7(3):544-56.
25. Saha RN, and Pahan K. Regulation of inducible nitric oxide synthase gene in glial cells. *Antioxid Redox Signal.* 2006;8(5-6):929-47.
26. Corbett GT, Gonzalez FJ, and Pahan K. Activation of peroxisome proliferator-activated receptor alpha stimulates ADAM10-mediated proteolysis of APP. *Proc Natl Acad Sci U S A.* 2015;112(27):8445-50.
27. Oakley H, Cole SL, Logan S, Maus E, Shao P, Craft J, et al. Intraneuronal beta-amyloid aggregates, neurodegeneration, and neuron loss in transgenic mice with five familial Alzheimer's disease mutations: potential factors in amyloid plaque formation. *J Neurosci.* 2006;26(40):10129-40.
28. Mondragon-Rodriguez S, Perry G, Luna-Munoz J, Acevedo-Aquino MC, and Williams S. Phosphorylation of tau protein at sites Ser(396-404) is one of the earliest events in Alzheimer's disease and Down syndrome. *Neuropathol Appl Neurobiol.* 2014;40(2):121-35.
29. Regan P, Piers T, Yi JH, Kim DH, Huh S, Park SJ, et al. Tau phosphorylation at serine 396 residue is required for hippocampal LTD. *J Neurosci.* 2015;35(12):4804-12.
30. Kanno T, Tsuchiya A, and Nishizaki T. Hyperphosphorylation of Tau at Ser396 occurs in the much earlier stage than appearance of learning and memory disorders in 5XFAD mice. *Behav Brain Res.* 2014;274:302-6.

31. Liu Y, Yin H, Zhao M, and Lu Q. TLR2 and TLR4 in autoimmune diseases: a comprehensive review. *Clin Rev Allergy Immunol.* 2014;47(2):136-47.
32. Oliveira-Nascimento L, Massari P, and Wetzler LM. The Role of TLR2 in Infection and Immunity. *Front Immunol.* 2012;3:79.
33. Reed-Geaghan EG, Savage JC, Hise AG, and Landreth GE. CD14 and toll-like receptors 2 and 4 are required for fibrillar A{beta}-stimulated microglial activation. *J Neurosci.* 2009;29(38):11982-92.
34. Yu JT, Mou SM, Wang LZ, Mao CX, and Tan L. Toll-like receptor 2 -196 to -174 del polymorphism influences the susceptibility of Han Chinese people to Alzheimer's disease. *J Neuroinflammation.* 2011;8:136.
35. Zhang W, Wang LZ, Yu JT, Chi ZF, and Tan L. Increased expressions of TLR2 and TLR4 on peripheral blood mononuclear cells from patients with Alzheimer's disease. *J Neurol Sci.* 2012;315(1-2):67-71.
36. Balayssac S, Burlina F, Convert O, Bolbach G, Chassaing G, and Lequin O. Comparison of penetratin and other homeodomain-derived cell-penetrating peptides: interaction in a membrane-mimicking environment and cellular uptake efficiency. *Biochemistry.* 2006;45(5):1408-20.
37. Borrelli A, Tornesello AL, Tornesello ML, and Buonaguro FM. Cell Penetrating Peptides as Molecular Carriers for Anti-Cancer Agents. *Molecules.* 2018;23(2).
38. Bera S, Kar RK, Mondal S, Pahan K, and Bhunia A. Structural Elucidation of the Cell-Penetrating Penetratin Peptide in Model Membranes at the Atomic Level: Probing Hydrophobic Interactions in the Blood-Brain Barrier. *Biochemistry.* 2016;55(35):4982-96.
39. Richard KL, Filali M, Prefontaine P, and Rivest S. Toll-like receptor 2 acts as a natural innate immune receptor to clear amyloid beta 1-42 and delay the cognitive decline in a mouse model of Alzheimer's disease. *J Neurosci.* 2008;28(22):5784-93.
40. Friis LM, Keelan M, and Taylor DE. Campylobacter jejuni drives MyD88-independent interleukin-6 secretion via Toll-like receptor 2. *Infect Immun.* 2009;77(4):1553-60.
41. Gao Q, Qi L, Wu T, and Wang J. Clostridium butyricum activates TLR2-mediated MyD88-independent signaling pathway in HT-29 cells. *Mol Cell Biochem.* 2012;361(1-2):31-7.
42. Buggia-Prevot V, Sevalle J, Rossner S, and Checler F. NFkappaB-dependent control of BACE1 promoter transactivation by Abeta42. *J Biol Chem.* 2008;283(15):10037-47.
43. Atri A. Effective pharmacological management of Alzheimer's disease. *Am J Manag Care.* 2011;17 Suppl 13:S346-55.
44. Bennett DA, Schneider JA, Arvanitakis Z, Kelly JF, Aggarwal NT, Shah RC, et al. Neuropathology of older persons without cognitive impairment from two community-based studies. *Neurology.* 2006;66(12):1837-44.
45. Bennett DA, Schneider JA, Arvanitakis Z, and Wilson RS. Overview and findings from the religious orders study. *Curr Alzheimer Res.* 2012;9(6):628-45.
46. Bennett DA, Schneider JA, Bienias JL, Evans DA, and Wilson RS. Mild cognitive impairment is related to Alzheimer disease pathology and cerebral infarctions. *Neurology.* 2005;64(5):834-41.
47. Wilson RS, Beckett LA, Barnes LL, Schneider JA, Bach J, Evans DA, et al. Individual differences in rates of change in cognitive abilities of older persons. *Psychol Aging.* 2002;17(2):179-93.
48. Braak H, and Braak E. Neuropathological stageing of Alzheimer-related changes. *Acta Neuropathol.* 1991;82(4):239-59.
49. Jana A, Modi KK, Roy A, Anderson JA, van Breemen RB, and Pahan K. Up-regulation of neurotrophic factors by cinnamon and its metabolite sodium benzoate: therapeutic implications for neurodegenerative disorders. *J Neuroimmune Pharmacol.* 2013;8(3):739-55.

50. Corbett GT, Roy A, and Pahan K. Gemfibrozil, a lipid-lowering drug, upregulates IL-1 receptor antagonist in mouse cortical neurons: implications for neuronal self-defense. *J Immunol.*189(2):1002-13.
51. Khasnavis S, and Pahan K. Sodium benzoate, a metabolite of cinnamon and a food additive, upregulates neuroprotective Parkinson disease protein DJ-1 in astrocytes and neurons. *J Neuroimmune Pharmacol.* 2012;7(2):424-35.
52. Roy A, Jana M, Kundu M, Corbett GT, Rangaswamy SB, Mishra RK, et al. HMG-CoA Reductase Inhibitors Bind to PPARalpha to Upregulate Neurotrophin Expression in the Brain and Improve Memory in Mice. *Cell Metab.* 2015;22(2):253-65.
53. Roy A, Kundu M, Jana M, Mishra RK, Yung Y, Luan CH, et al. Identification and characterization of PPARalpha ligands in the hippocampus. *Nat Chem Biol.* 2016;12(12):1075-83.
54. Mondal S, Martinson JA, Ghosh S, Watson R, and Pahan K. Protection of Tregs, suppression of Th1 and Th17 cells, and amelioration of experimental allergic encephalomyelitis by a physically-modified saline. *PLoS ONE.* 2012;7(12):000.
55. Mondal S, and Pahan K. Cinnamon ameliorates experimental allergic encephalomyelitis in mice via regulatory T cells: implications for multiple sclerosis therapy. *PLoS One.* 2015;10(1):e0116566.
56. Pike CJ, Burdick D, Walencewicz AJ, Glabe CG, and Cotman CW. Neurodegeneration induced by beta-amyloid peptides in vitro: the role of peptide assembly state. *J Neurosci.* 1993;13(4):1676-87.
57. Roy A, Jana M, Corbett GT, Ramaswamy S, Kordower JH, Gonzalez FJ, et al. Regulation of cyclic AMP response element binding and hippocampal plasticity-related genes by peroxisome proliferator-activated receptor alpha. *Cell Rep.* 2013;4(4):724-37.
58. Mansuy IM, Mayford M, Jacob B, Kandel ER, and Bach ME. Restricted and regulated overexpression reveals calcineurin as a key component in the transition from short-term to long-term memory. *Cell.* 1998;92(1):39-49.
59. Khasnavis S, Roy A, Ghosh S, Watson R, and Pahan K. Protection of dopaminergic neurons in a mouse model of Parkinson's disease by a physically-modified saline containing charge-stabilized nanobubbles. *J Neuroimmune Pharmacol.* 2013;9(2):218-32.

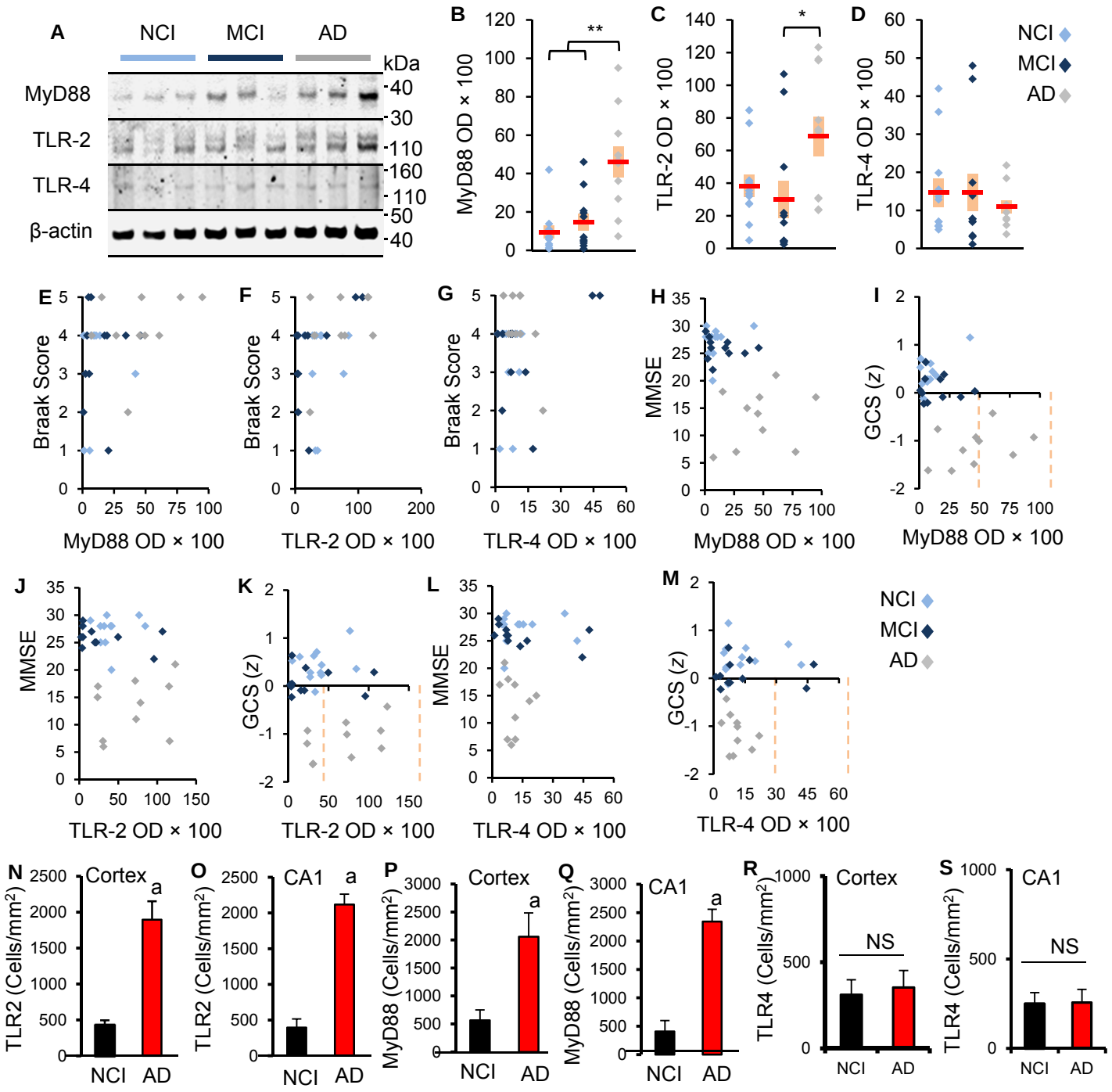

Figure 1. Monitoring levels of TLR2, TLR4 and MyD88 in the CNS of cases clinically diagnosed as no cognitive impairment (NCI), mild cognitive impairment (MCI,) and Alzheimer's disease (AD). (A) Pre-frontal cortex homogenates (25µg) from NCI (light blue), MCI (dark blue) and AD (grey) were immunoblotted for TLR2, TLR4 and MyD88. Actin was used to normalize signals obtained by densitometric measurement (NIH ImageJ). Coomassie was used to verify protein loading. Twelve NCI, eleven MCI and ten AD cases were run in three independent experiments. MyD88 (B) was significantly elevated in AD relative to both NCI ($p < .001$) and MCI ($p < .001$). TLR2 (C) was significantly higher in AD compared with MCI subjects ($p < .05$) by Kruskal-Wallis test. TLR4 (D) did not differ significantly across the three groups. MyD88 (E; .371, p = .033) and TLR2 (F; .463, p = .007) positively correlated with Braak score by Kruskal-Wallis test. No such correlation was found between TLR4 (G; -.012, p = .947) and Braak score. MyD88 negatively correlated with Mini-Mental State Examination (MMSE) scores (H; -.538, $p = .001$) and global cognitive z score (GCS) index (I; -.475, $p = -.005$). However, the negative correlation was not significant for TLR2 with MMSE (J; -.278, p = .117) and GCS (K; -.177, p = .326). TLR4 was also not negatively correlated with MMSE (L; -.173, p = .336) and GCS (M; .047, p = .794). kDa, kilodalton; OD, optical density. Hippocampal sections of NCI and AD brains were double-labeled with Iba-1 (microglia) and TLR2, TLR4 or MyD88. Cells positive for TLR2 (N, cortex; O, CA1), MyD88 (P, cortex; Q, CA1) and TLR4 (R, cortex; S, CA1) were counted in two sections (two images per slide) of each of four different cases. [a]*p < 0.001 vs NCI* by two-sample t-tests. *NS, not significant.*

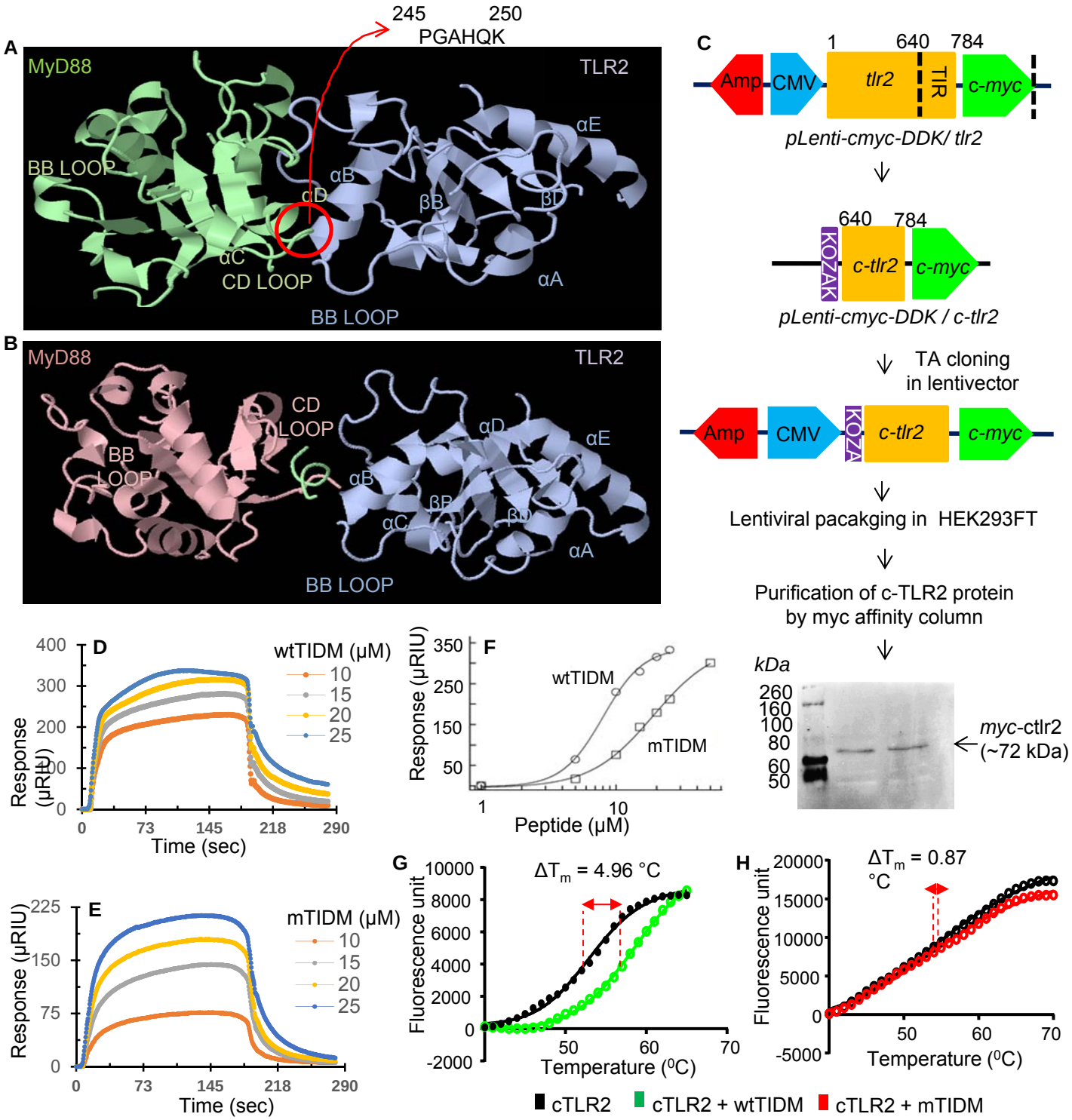

Figure 2. Designing a peptide for disruption of TLR2 and MyD88 interaction. (A) A rigid-body *in silico* docked pose of mouse TLR2 (blue) and MyD88 (green) (electrostatic energy = -7.750 KCal/mol; desolvation energy = -24.99 Kcal/mol; VDW energy = 105.25 Kcal/mol; Total energy = -22.216 KCal/mol) shows strong interaction between 245 to 250 amino acid of the CD loop of MyD88 and the BB loop of TLR2. Therefore, peptide corresponding to this domain of MyD88 (TIDM) was used to dissociate the interaction between TLR2 and MyD88. B) TLR2-MyD88 interaction was complexed with wtTIDM peptide (electrostatic energy = -4.516 KCal/mol; desolvation energy = -24.027 KCal/mol; VDW energy = 16.724 KCal/mol; Total energy= -26.871 KCal/mol). C) Generation of cMyc-tagged C-terminal TLR2 (cTLR2) recombinant protein. The *in vitro* binding affinity of increasing doses of wtTIDM (D) and mTIDM (E) with cTLR2 was examined using surface plasmon resonance analyses (n=2 replicates/dose in 3 independent experiments). F) Plot of the binding response values versus the concentrations of wtTIDM (circle) and mTIDM (square) peptides. G) Melting curve of cTLR2 protein (black) alone and with wtTIDM (green). Thermal shift analyses showed 4.96°C shift (ΔTm) of melting temperature (n=2 replicates/dose in 3 independent experiments). H) Melting curve of cTLR2 protein (black) alone and with mTIDM peptides (red) indicated a ΔTm of 0.87°C (n=2 replicates/dose in 3 independent experiments).

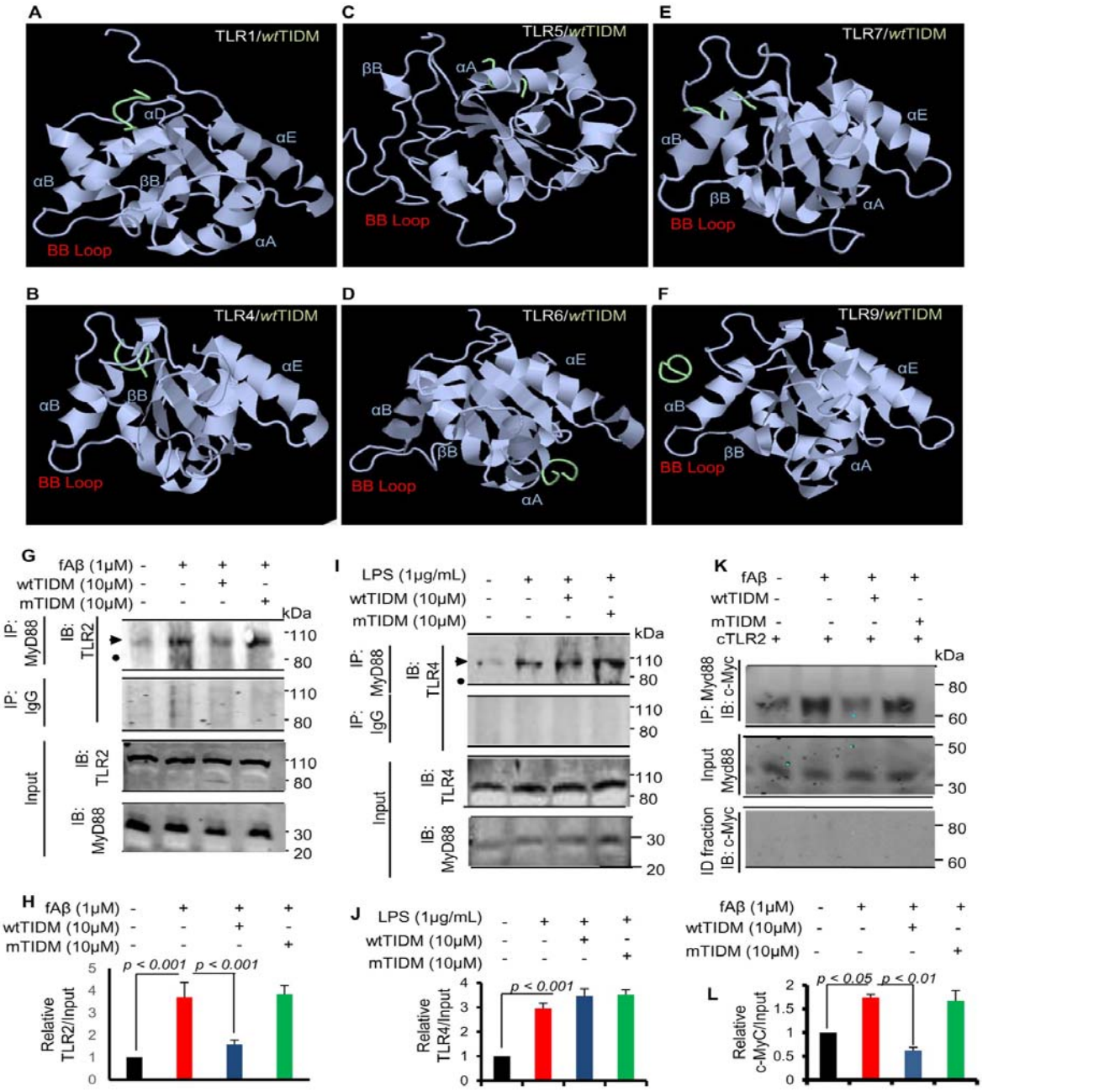

Figure 3. Selective disruption of TLR2 and MyD88 interaction by wtTIDM. *In silico* analyses of interactions of wtTIDM with TLR1, TLR4, TLR5, TLR6, TLR7, and TLR9. A rigid body interaction analyses were performed in pydock in silico analysis tool. Complexes of TLR1-wtTIDM (A), TLR4-wtTIDM (B), TLR5-wtTIDM (C), TLR6-wtTIDM (D), TLR7-wtTIDM (E), and TLR9-wtTIDM (F) were displayed. G) BV-2 microglial cells preincubated with wtTIDM and mTIDM peptides for 1 h were stimulated with 1 μM fibrillar Aβ1-42 under serum-free condition. After 1 h, cellular extracts were immunoprecipitated with anti-MyD88 antibody followed by western blot of immunoprecipitates for TLR2. As control, cellular extracts were immunoprecipitated with normal IgG. Input was also immunoblotted with TLR2 and MyD88. H) Bands were scanned and values (TLR2/Input) presented as relative to control (n=2 replicates/condition in 3 independent experiments). Results were analyzed by two-sample t-tests. I) BV-2 microglial cells preincubated with wtTIDM and mTIDM peptides for 1 h were stimulated with LPS under serum-free condition. After 1 h, cellular extracts were immunoprecipitated with anti-MyD88 antibody followed by western blot of immunoprecipitates for TLR4. As control, cellular extracts were immunoprecipitated with normal IgG. Input was also immunoblotted with TLR4 and MyD88. J) Bands were scanned and values (TLR4/Input) presented as relative to control (n=2 replicates/condition in 3 independent experiments). Results were analyzed by two-sample t-tests. K) BV-2 microglial cells were transduced with *pLenti-cMyc-cTlr2* lentivirions and 48 h after transduction, cells were treated with wtTIDM and mTIDM for 1 h followed by stimulation with fibrillar Aβ1-42. After 1 h, cellular extracts were immunoprecipitated with anti-MyD88 antibody followed by western blot of immunoprecipitates for c-Myc. Immuno-depleted (ID) fractions were also immunoblotted for c-Myc as control. L) Bands were scanned and values (c-Myc/Input) presented as relative to control (n=2 replicates/condition in 3 independent experiments). Results were analyzed by two-sample t-tests.

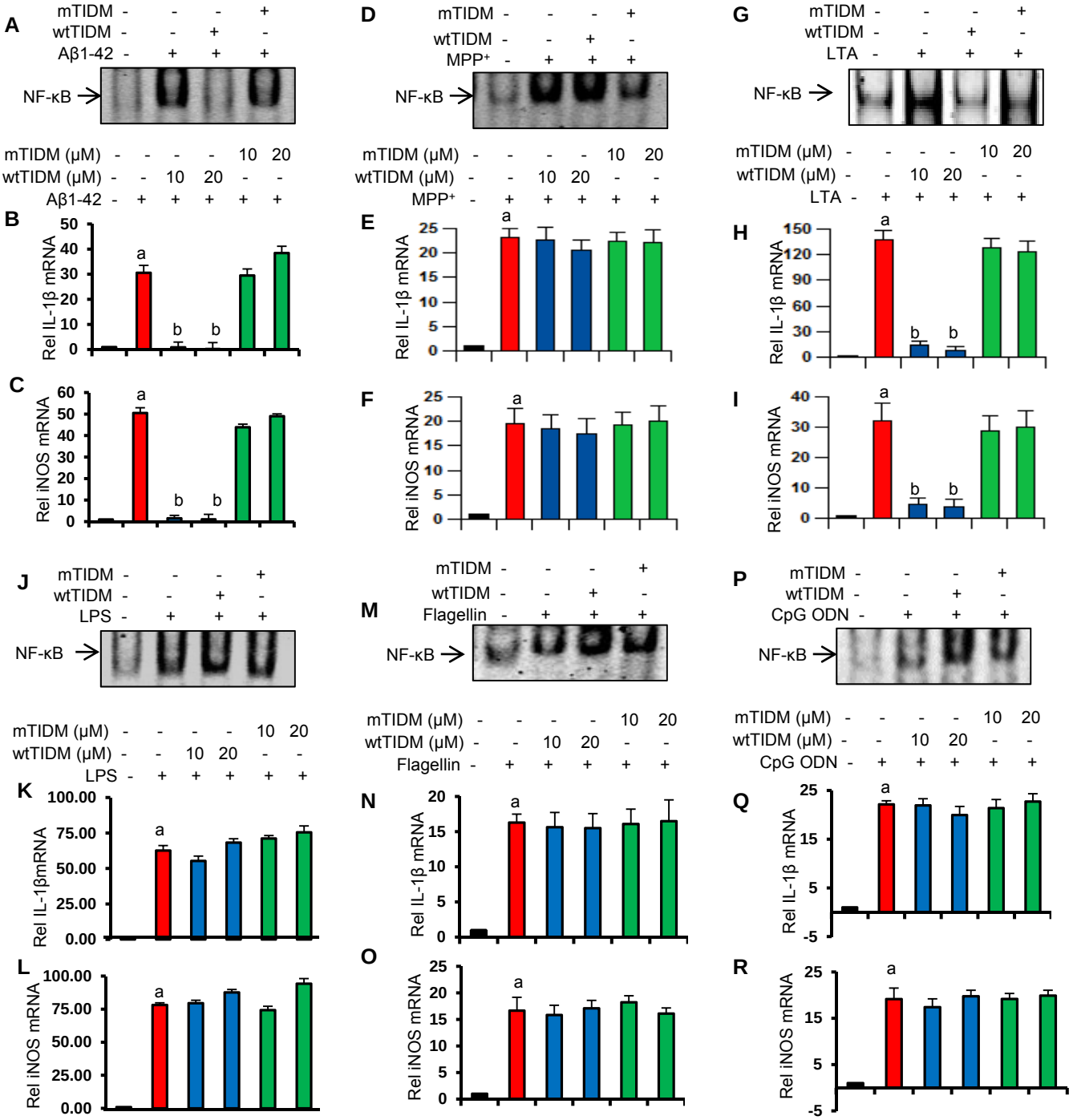

Figure 4. Effect of wtTIDM and mTIDM peptides on the induction of NF-κB activation and the expression of proinflammatory molecules in microglial cells. BV-2 microglial cells preincubated with 10 μM wtTIDM/mTIDM peptides for 1 h were stimulated with 1 μM fibrillar Aβ1-42 (A-C), 1 μM MPP^+ (D-F), 250 ng/ml LTA (G-I), 1 μg/ml LPS (J-L), 1 μM flagellin (M-O), and 1 μM CpG DNA (P-R) under serum-free condition. After 1 h of stimulation, the activation of NF-κB was monitored in nuclear extracts by EMSA (A, fibrillar Aβ; D, MPP^+; G, LTA; J, LPS; M, flagellin, P; CpG DNA). After 4 h of stimulation, the mRNA expression of IL-1β (B, E, H, K, N, & Q) and iNOS (C, F, I, L, O, & R) was monitored by real-time PCR (B-C, fibrillar Aβ; E-F, MPP^+; H-I, LTA; K-L, LPS; N-O, flagellin; Q-R, CpG DNA) (n=2 replicates/dose in 3 independent experiments). $^a p < 0.001$ *vs control;* $^b p < 0.001$ *vs stimuli* by two-sample t-tests.

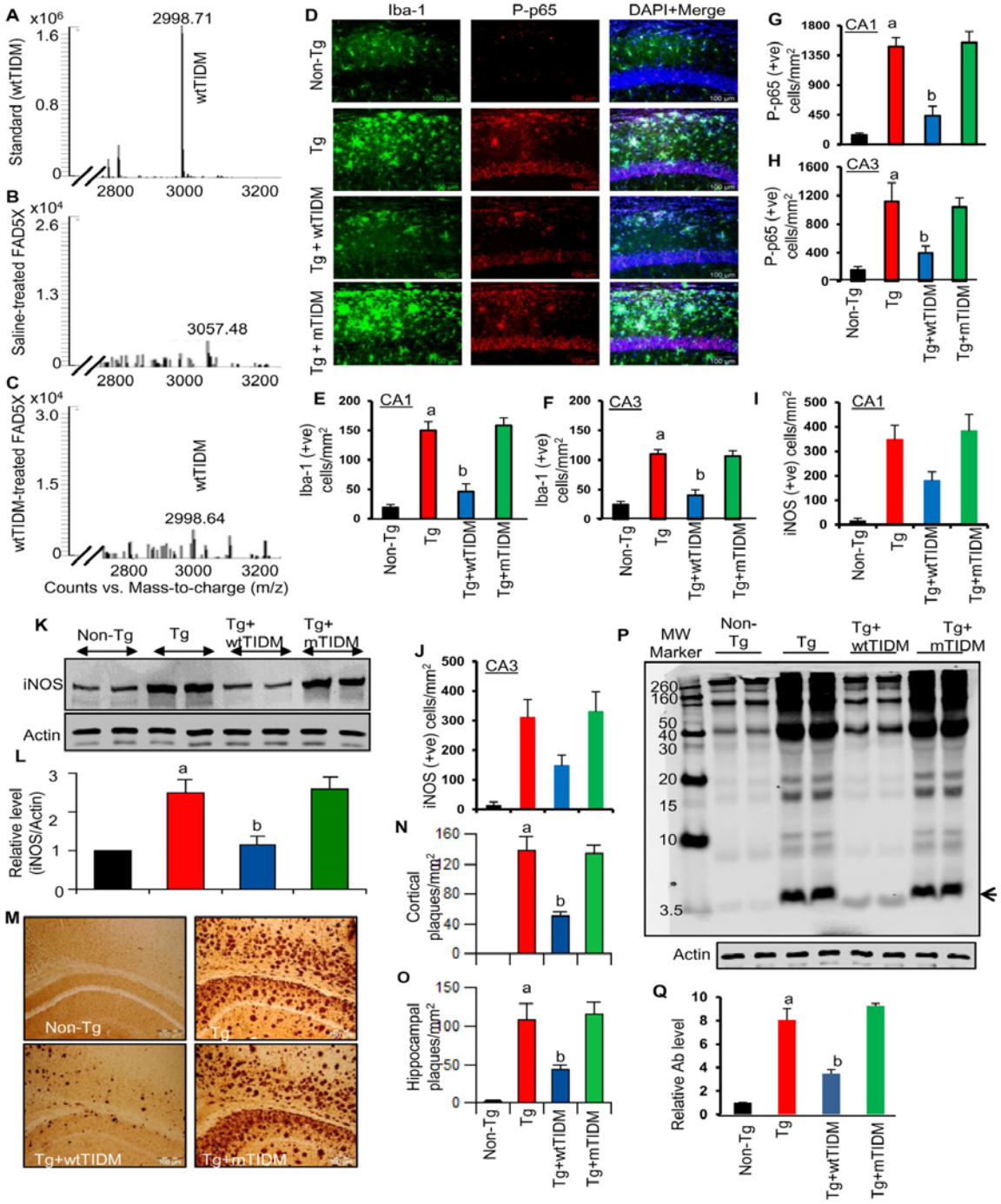

Figure 5. After intranasal delivery, wtTIDM peptide enters into the hippocampus and suppresses glial activation and reduces plaques in the hippocampus of Tg mice. Tg mice (6-month old) received one dose of wtTIDM peptide (0.1 mg/kg body wt) via intranasal route. After 60 min of treatment, mice were perfused with sterile saline and hippocampi were homogenized and supernatant was analyzed for wtTIDM by electrospray ionization-coupled mass spectrometry (ESI-MS) (A, wtTIDM standard; B, untreated Tg; C, wtTIDM-treated Tg). Tg mice were treated with wtTIDM and mTIDM peptides (0.1 mg/kg body wt/2d) via intranasal route. After 30d, hippocampal sections were double-labeled for Iba-1 & P-p65 (D) and Iba-1 & iNOS (Fig. S9). Cells positive for Iba-1 (E, CA1; F, CA3), P-p65 (G, CA1; H, CA3) and iNOS (I, CA1; J, CA3) were counted in two sections (two images per slide) of each of six different mice (n=6) per group. $^{a}p < 0.001$ *vs non-Tg;* $^{b}p < 0.001$ *vs Tg* by two-sample t-tests. Hippocampal extracts of all groups of mice (n=4 per group) were immunoblotted for iNOS (K). Actin was run as loading control. Bands were scanned and values (L, iNOS/Actin) presented as relative to non-Tg control. $^{a}p < 0.001$ *vs non-Tg;* $^{b}p < 0.001$ *vs Tg* by two-sample t-tests. M) Hippocampal sections were immunolabeled with 82E1 mAb. Amyloid plaques (N, cortex; O, hippocampus) were counted in two sections (two images per slide) of each of six different mice per group. $^{a}p < 0.001$ *vs non-Tg;* $^{b}p < 0.001$ *vs Tg* by two-sample t-tests. P) Hippocampal extracts (n=4 per group) were analyzed for Aβ by Western blot using 6E10 mAb. Arrowhead indicates 4 kDa Aβ band. Bands were scanned and values (Aβ/Actin) presented as relative to non-Tg control (Q). $^{a}p < 0.001$ *vs non-Tg;* $^{b}p < 0.001$ *vs Tg* by two-sample t-tests.

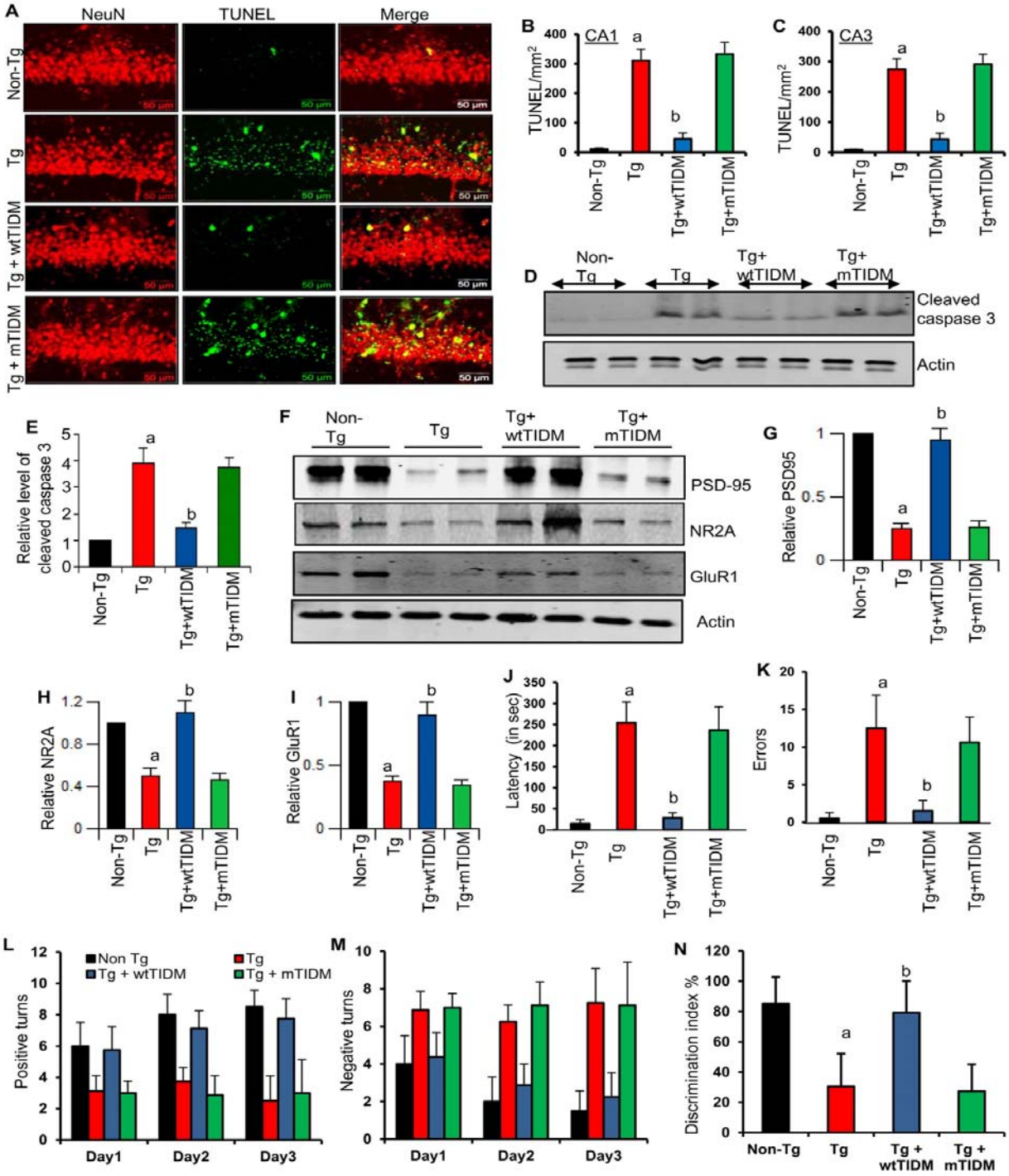

Figure 6. Intranasal delivery of wtTIDM, but not mTIDM, peptide inhibits neuronal apoptosis *in vivo* in the hippocampus and improves memory and learning in Tg mice. Tg mice (6-month old) were treated with wtTIDM and mTIDM peptides (0.1 mg/kg body wt/2d) via intranasal route. After 30 d of treatment, mice were sacrificed and hippocampal sections were double-labeled for TUNEL & NeuN (A). TUNEL-positive cells (B, CA1; C, CA3) were counted in two sections (two images per slide) of each of six different mice (n=6) per group. $^{a}p < 0.001$ *vs non-Tg;* $^{b}p < 0.001$ *vs Tg* by two-sample t-tests. Hippocampal extracts of all groups of mice (n=4) were immunoblotted for cleaved caspase 3 (D). Actin was run as loading control. E) Bands were scanned and values (cleaved caspase 3/Actin) are presented as relative to non-Tg control. Results are expressed as mean ± SEM of four mice per group. $^{a}p < 0.001$ *vs non-Tg;* $^{b}p < 0.001$ *vs Tg* by two-sample t-tests. Protein levels of PSD-95, NR2A and GluR1 were monitored in hippocampal extracts by Western blot (F). Bands were scanned and values (G, PSD-95/Actin; H, NR2A/Actin; I, GluR1/Actin) are presented as relative to non-Tg control. Results are expressed as mean ± SEM of four mice per group. $^{a}p < 0.001$ *vs non-Tg;* $^{b}p < 0.001$ *vs Tg* by two-sample t-tests. Mice were tested for Barnes maze (J, latency; K, number of errors made) and T maze (L, number of positive turns; M, number of negative turns). Short-term memory was also monitored by novel object recognition test, which is represented by discrimination index (N). Eight mice (n=8) were used in each group and results were analyzed by one-way ANOVA.

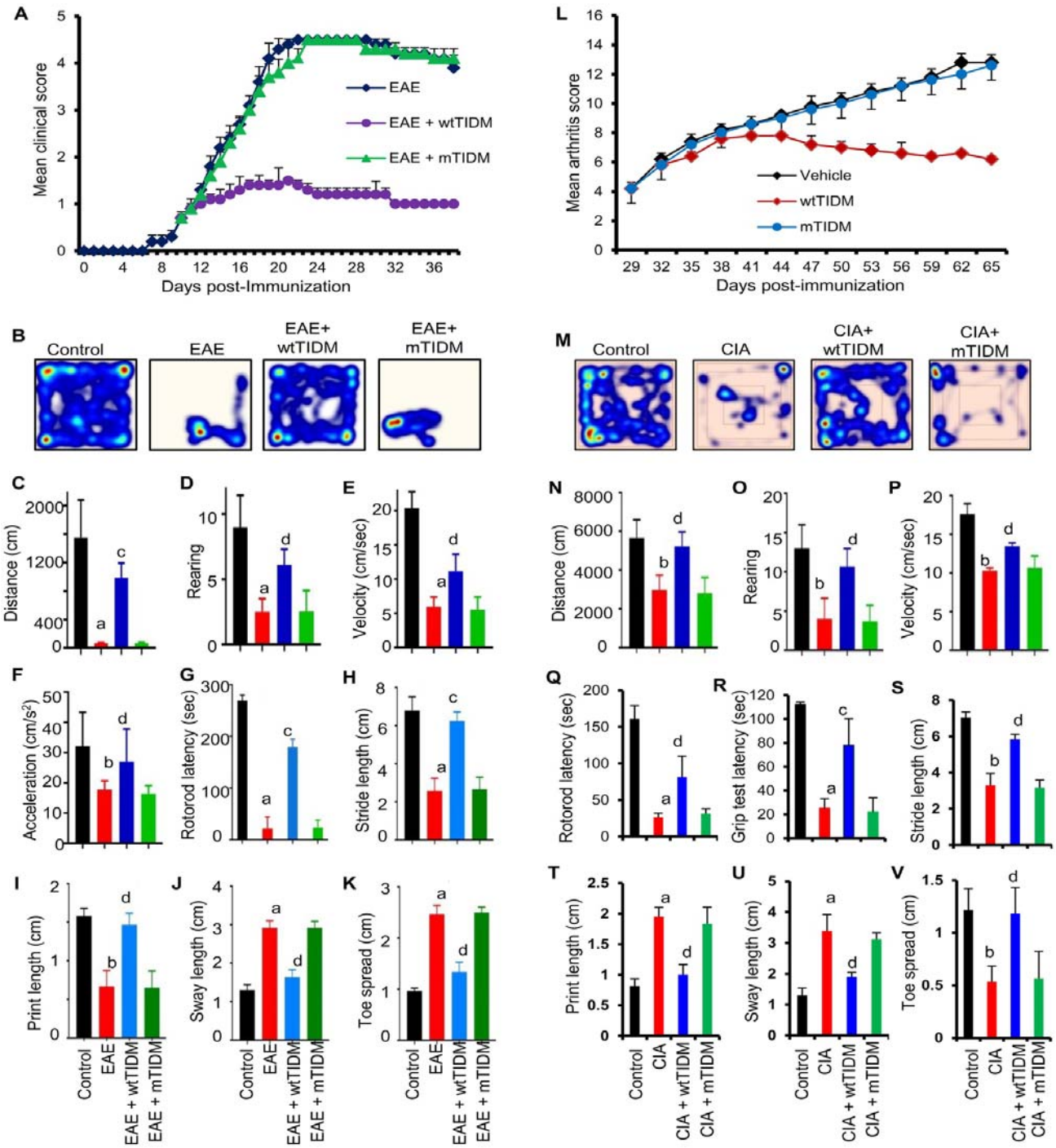

Figure 7. The wtTIDM, but not mTIDM, peptide protects mice from experimental allergic encephalomyelitis (EAE) and collagen-induced arthritis (CIA). A) EAE was induced in male C57/BL6 mice by MOG35-55 immunization and from 10 dpi, mice were treated with wtTIDM and mTIDM peptides (0.1 mg/kg body wt/d) via intranasal route. Mice (n=6 per group in two independent experiments) were scored daily. As evident by one-way repeated-measures ANOVA, the wtTIDM peptide significantly protected EAE [$F_{2, 94}$ = 22.59(>Fc = 3.093)]. On 22 dpi, general motor activities were monitored using the Ethovision XT 13.0 Open Field Activity System (Noldus) (B, heat-map images representing overall motor activities; C, distance travelled; D, rearing; E, velocity; F, acceleration) and rotorod (G). Foot print analysis (H, stride length; I, print length; J, sway length; K, toe spread) was also performed. L) CIA was induced in male DBA/1J mice by bovine type II collagen immunization and from 29 dpi, mice were treated with wtTIDM and mTIDM peptides (1 mg/kg body wt/d) via i.p. injection. Mice (n=6 per group in two independent experiments) were scored daily. One-way repeated-measures ANOVA shows that the wtTIDM peptide significantly protected CIA [$F_{2, 45}$ = 4.927(>Fc = 3.093)]. On 60 dpi, general motor activities were monitored by Ethovision System (M, heat-map images representing overall motor activities; N, distance travelled; O, rearing; P, velocity), rotorod (Q) and grip strength (R). Foot print analysis (S, stride length; T, print length; U, sway length; V, toe spread) was also performed. Six mice (n=6 per group) were used in two independent experiments. *$^{a}p < 0.001$ & $^{b}p < 0.05$ vs control; $^{c}p < 0.001$ & $^{d}p < 0.05$ vs EAE or CIA* by two-sample t-tests.